

PERTURBED FACTOR ANALYSIS: IMPROVING GENERALIZABILITY ACROSS STUDIES

BY ARKAPRAVA ROY^{*}, ISAAC LAVINE[†], AMY H. HERRING[†] AND DAVID
B. DUNSON[†]

^{}University of Florida, [†]Duke University*

Factor analysis is routinely used for dimension reduction. However, a major issue is the tendency to obtain substantially different factors in analyzing similar datasets. Factor models have been developed for multi-group data by using additive expansions incorporating common and group-specific factors. However, allowing group-specific factors runs counter to the goal of producing a single set of factors that hold across groups. As an alternative, we propose a class of Perturbed Factor Analysis (PFA) models that assume a common factor structure after perturbing the data via multiplication by a group-specific matrix. Bayesian inference algorithms are defined using a matrix normal hierarchical model for the perturbation matrices. The resulting model is just as flexible as current approaches in allowing arbitrarily large differences across groups, but has substantial advantages that we illustrate in simulation studies and our application to NHANES data. We additionally show advantages of PFA in single group data analyses in which we assign each individual their own perturbation matrix, including reduced generalization error and improved identifiability.

1. Introduction. Exposures to phthalates are ubiquitous. They are present in soft plastics, including vinyl floors, toys and food packaging. Medical supplies such as blood bags and tubes contain phthalates. They are also found in fragrant products such as soap, shampoo, lotion, perfume and scented cosmetics. There is substantial interest in studying levels of exposure of people in different groups to phthalates, and in relating these exposures to health effects. This has motivated the collection of phthalate concentration data in urine in the National Health and Nutrition Examination Survey (NHANES) (<https://www.cdc.gov/nchs/nhanes>). When they enter the body, phthalate parent compounds are broken down into different metabolites; assays measuring phthalate exposures target these different breakdown products. As these chemicals are often moderately to highly correlated, it is common to identify a small set of underlying factors (for example [Weissenburger-Moser et al. \(2017\)](#)). Epidemiologists are interested

Keywords and phrases: Bayesian, Factor analysis, Generalizability, Hierarchical model, Meta analysis, Perturbation matrix, Robustness

in interpreting these factors and in using them in analyses relating exposures to health outcomes.

However, many research groups have noticed a tendency to estimate very different factors in applying factor analysis to similar datasets or groups of individuals. For example, [Maresca et al. \(2016\)](#) examined data from three children’s cohorts and noted marked differences in factor structure in one of them. [James-Todd et al. \(2017\)](#) found variation in phthalate exposure patterns of pregnant women by race. [Bloom et al. \(2019\)](#) noted differences in both phthalate exposures and in associations with birth outcome by race. Certainly, we would like to allow for possible differences in exposures across groups; indeed, studying such differences is one of our primary interests. Such differences may relate to questions of environmental justice and may partly explain differences with ethnicity in numerous health outcomes. However, even though the levels and specific sources of phthalate exposures may vary across groups, there is no reason to suspect that the fundamental relationship between levels of metabolites and latent factors would differ. Such differences in the factor structure are more likely to arise due to statistical uncertainty and sensitivity to slight differences in the data and can greatly complicate inferences on similarities and differences across groups.

To set the stage to discuss factor modeling of multi-group data, consider a typical factor model for p -variate data $Y_i = (Y_{i1}, \dots, Y_{ip})^T$ from a single group:

$$(1.1) \quad Y_i = \Lambda \eta_i + \epsilon_i, \quad \eta_i \sim \text{MVN}(0, I_k), \quad \epsilon_i \sim \text{MVN}(0, \Sigma),$$

where it is assumed that data are centered prior to analysis, $\eta_i = (\eta_{i1}, \dots, \eta_{ik})^T$ are latent factors, Λ is a $p \times k$ factor loadings matrix, and $\Sigma = \text{diag}(\sigma_1^2, \dots, \sigma_p^2)$ is a diagonal matrix of residual variances. Under this model, marginalizing out the latent factors η_i induces the covariance $H = \text{cov}(Y_i) = \Lambda \Lambda^T + \Sigma$.

To extend (1.1) to data from multiple groups, most of the focus has been on decomposing the covariance into shared and group-specific components. A key contribution was JIVE (Joint and Individual Variation Explained), which identifies low-rank covariance structure that is shared among multiple data types collected for the same subject ([Lock et al., 2013](#); [Feng, Hannig and Marron, 2015](#); [Feng et al., 2018](#)). In a Bayesian framework, [Roy, Schaich-Borg and Dunson \(2019\)](#) proposed TACIFA (Time Aligned Common and Individual Factor Analysis) for a related problem. More directly relevant to our phthalate application are the multi-study factor analysis (MSFA) methods of [De Vito et al. \(2018, 2019\)](#). These approaches replace $\Lambda \eta_i$ in (1.1) with an additive expansion containing shared and group-specific components. [De Vito et al. \(2018\)](#) implement a Bayesian version of MSFA

(BMSFA), while [De Vito et al. \(2019\)](#) develop a frequentist implementation. [Kim et al. \(2018\)](#) propose a related approach using PCA.

The above methods are very useful in many applications, but do not address our goal of improving inferences in our phthalate application by obtaining a common factor representation that holds across groups. In addition, we find that additive expansions can face issues with weak identifiability - the model can fit the data well by decreasing the contribution of the shared component and increasing that of the group-specific components; this issue can lead to slower convergence and mixing rates for sampling algorithms for implementing BMSFA and potentially higher estimation errors in estimating the component factor loadings matrices.

We aim to identify a single set of factors under the assumption that the data in each group can be aligned to a common latent space via multiplication by a perturbation matrix. We represent the perturbed covariance in group j as $Q_j \Sigma Q_j^T$, where Σ is the common covariance, and Q_j is the group-specific perturbation matrix. As in the common factor model in (1.1), the overall covariance Σ can be decomposed into a component due to common factors and a residual variance. The utility of the perturbation model also extends beyond multi-group settings. In the common factor model, the error terms only account for additive measurement error. We can obtain robust estimates of factor loadings in a single dataset by allowing for observation-specific perturbations. This accounts for both multiplicative and additive measurement error. In this case, we define separate Q_i 's for each data vector Y_i . Here Q_i 's are multiplicative random effects with mean I_p . Thus, $E(Q_i Y_i) = E(Y_i)$ and the covariance structure on Q_i would determine the variability of $Q_i Y_i$.

We take a Bayesian approach to inference using Markov chain Monte Carlo (MCMC) for posterior sampling, related to [De Vito et al. \(2018\)](#) but using our Perturbed Factor Analysis (PFA) approach instead of their additive BMSFA model. Model (1.1) faces well known issues with non-identifiability of the loadings matrix Λ ([Seber, 2009](#); [Lopes and West, 2004](#); [Ročková and George, 2016](#); [Fruehwirth-Schnatter and Lopes, 2018](#)); this non-identifiability problem is inherited by multiple group extensions such as BMSFA. It is very common in the literature to run MCMC ignoring the identifiability problem and then post-process the samples. [Aßmann, Boysen-Hogrefe and Pape \(2016\)](#); [McParland et al. \(2014\)](#) obtain a post-processed estimate by solving an orthogonal Procrustes problem, but without uncertainty quantification (UQ). [Roy, Schaich-Borg and Dunson \(2019\)](#) post-process the entire MCMC chain iteratively to draw inference with UQ. [Lee, Lin and McLachlan \(2018\)](#) instead address non-identifiability by giving

the latent factors non-symmetric distributions, such as half-t or generalized inverse Gaussian. We instead choose heteroscedastic latent factors to remove rotational ambiguity in the loadings matrix, except for permutations. We find this approach can also improve accuracy in estimating the covariance, perhaps due to the flexible shrinkage prior that is induced.

The next section describes the data and the model in detail. In Section 3, prior specifications are discussed. Our computational scheme is outlined in Section 4. We study the performance of our method in different simulation setups in Section 5. Section 6 considers an application to NHANES data. We end with some concluding remarks in Section 7.

2. Data description and modeling. We focus on data from the National Health and Nutrition Examination Survey (NHANES) because the study is population-representative yet also allows examination of phthalates across subgroups related to health risks and susceptibility. We have data on chemical levels in urine recorded over the span 2009 to 2013 for 2749 individuals. We consider in total eight phthalate metabolite chemicals, Mono-n-butyl (MnBP), Mono-isobutyl (MiBP), Mono-ethyl (MEP), Mono-benzyl (MBeP), Mono-2-ethyl-5-carboxypentyl (MECPP), Mono-(2-ethyl-5-hydroxyhexyl) (MEHHP), Mono-(2-ethyl-5-oxohexyl) (MEOHP) and Mono-(2-ethyl)-hexyl (MEHP), measured in participants identified with racial and ethnic groups Mexican American (Mex), Other Hispanic (OH), Non-Hispanic White (N-H White), Non-Hispanic Black (N-H Black) and Other Race (Other/Multi) - Including Multi-Racial. We consider race and ethnicity because previous work has shown differences in patterns of use of products that contain phthalates (Taylor et al., 2018) and in measured phthalate concentrations (James-Todd et al., 2017) across them. Recent work has also indicated exposure effects themselves may vary across these groupings (Bloom et al., 2019), but this may be difficult to disentangle if factors lack sufficient robustness and generalizability. Excess levels of phthalates in blood/urine have been linked to a variety of health outcomes, including obesity (Zhang et al., 2014; Kim and Park, 2014; Benjamin et al., 2017) and birth outcomes (Bloom et al., 2019).

We provide a summary of the average chemical level across different groups in Table 1. In Table 2, we compute Hotelling T^2 statistic between each pair of groups. As noted in Bloom et al. (2019), exposure levels were generally higher among non-whites. For each phthalate variable, we also fit a one-way ANOVA model to determine differences across the groups taking Mexican-Americans as baseline. The results are included in Tables 2-6 in the supplementary materials. For the majority of phthalates, concentrations

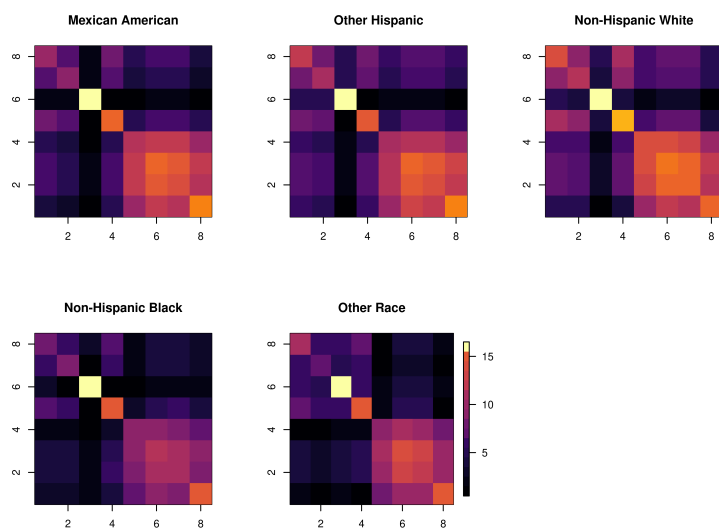


FIG 1. *Plots of the covariance matrices of the phthalate chemicals across different ethnic groups for NHANES data.*

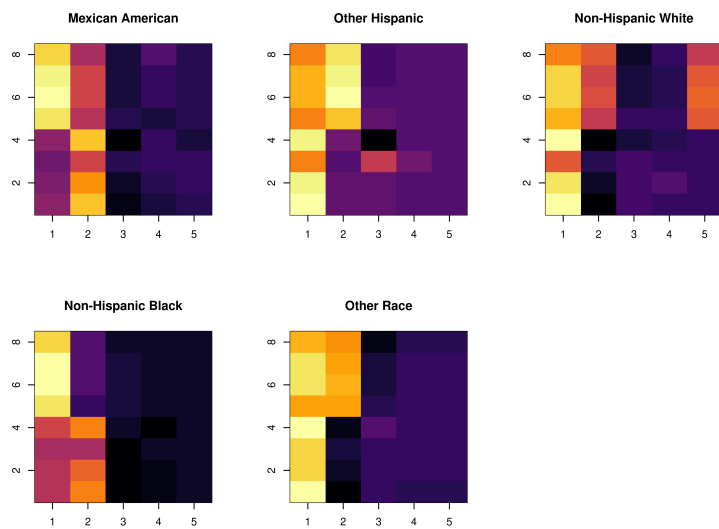


FIG 2. *Estimated loadings matrices for different ethnic groups based on applying separate Bayesian factor analyses using the approach of [Bhattacharya and Dunson \(2011\)](#).*

TABLE 1
Comparison across different groups in terms of number of participants and average chemical levels along with standard deviations in brackets.

	Mex	OH	N-H White	N-H Black	Other/Multi
Number of participants	566	293	1206	516	168
MnBP	3.85 (1.96)	4.31 (4.96)	3.56 (2.17)	4.21 (1.81)	3.76 (2.11)
MiBP	2.88 (1.36)	3.21 (1.70)	2.52 (1.20)	3.47 (1.67)	2.79 (1.21)
MEP	8.32 (6.64)	9.51 (6.99)	6.91 (5.43)	11.16 (9.38)	7.33 (7.57)
MBeP	2.79 (1.58)	2.78 (1.61)	2.70 (1.67)	3.06 (1.77)	2.56 (1.68)
MECPP	4.80 (3.68)	4.55 (2.68)	4.16 (2.40)	4.36 (2.38)	4.34 (2.64)
MEHHP	3.83 (3.01)	3.73 (2.59)	3.45 (2.25)	3.79 (2.26)	3.57 (2.45)
MEOHP	3.11 (2.41)	3.00 (1.92)	2.79 (1.69)	3.05 (1.71)	2.86 (1.86)
MEHP	1.58 (1.23)	1.59 (1.29)	1.33 (0.89)	1.61 (0.99)	1.58 (1.31)

TABLE 2
Hotelling T^2 statistic between phthalate levels for each pair of groups.

	Mex	OH	N-H White	N-H Black	Other/Multi
Mex	0.00	31.84	108.59	191.93	28.04
OH	31.84	0.00	156.45	63.48	28.69
N-H White	108.59	156.45	0.00	409.64	55.51
N-H Black	191.93	63.48	409.64	0.00	101.90
Other/Multi	28.04	28.69	55.51	101.90	0.00

are lowest among non-Hispanic whites. We plot group specific covariances in Figure 1. It is evident that there is shared structure with some differences across the groups, and the estimated loading matrices are different when we fit the common factor model in (1.1) separately for each group. In the next subsection, we propose a novel approach for multi-group factor analysis to identify the common factors.

2.1. *Multi-group model.* Assume that we observe data from multiple groups, with the groups corresponding to individuals in different racial and ethnic categories in NHANES. Each p -dimensional response Y_{ij} , belonging

to group G_j , for $j \in 1 : J$ and $i \in 1 : n_j$, is modeled as:

$$(2.1) \quad \begin{aligned} Q_j Y_{ij} &= \Lambda \eta_{ij} + \epsilon_{ij}, \\ Q_j &\sim \text{MN}_{p \times p}(I_p, U, V), \quad \eta_{ij} \sim N(0, E), \\ \epsilon_{ij} &\sim \text{MVN}(0, \Sigma). \end{aligned}$$

The perturbation matrices Q_j are of dimension $p \times p$, and follow a matrix normal distribution, with isotropic covariances $U = V = \alpha I_p$. The latent factors η_{ij} are heteroscedastic, so that E is diagonal with non-identical entries such that $E = \text{diag}(e_1, \dots, e_k)$ with k factors in the model and $\Sigma = \text{diag}(\sigma_1, \dots, \sigma_p)$. We discuss advantages of choosing heteroscedastic latent factors in more detail in Section 2.3. After integrating out the latent factors, observations are marginally distributed as $Y_{ij} \sim \text{MVN}(0, Q_j^{-1}[\Lambda E \Lambda^T + \Sigma](Q_j^{-1})^T)$. If we write $Q_j^{-1} = I_p + \Psi_j$, then Λ is the shared loadings matrix, and $\Psi_j \Lambda$ is a group-specific loadings matrix. We can quantify the magnitude of perturbation as $\|\Psi_j\|_F$, where $\|\cdot\|_F$ stands for the Frobenius norm. For identifiability of Q_j 's, we consider $Q_1 = I_p$ and $n_1 \geq 2$. We call our model Perturbed Factor Analysis (PFA).

2.1.1. *Model properties.* Let Ω_1 and Ω_2 be two positive definite (p.d.) matrices. Then there exist non-singular matrices A and B , where $\Omega_1 = AA^T$ and $\Omega_2 = BB^T$. By choosing $E = AB^{-1}$, we have $\Omega_1 = E\Omega_2 E^T$. If the two matrices Ω_1 and Ω_2 are close, then E will be close to the identity. However, E is not required to be symmetric. In our multi-group model in (2.1), the Q_j s allow for small perturbations around the shared covariance matrix $H = \Lambda E \Lambda^T + \Sigma$. We define the following class for the Q_j 's,

$$\mathcal{C}_\epsilon = \{Q : \|Q - I_p\|_F \leq \epsilon\}.$$

The index ϵ controls the amount of deviation across groups. In (2.1) we define $U = V = \alpha I_p$, for some small α , which we call the perturbation parameter. By choosing $U = V$ to be isotropic covariances, we impose uniform perturbation across all the rows and columns around I_p . However, the perturbation matrices themselves are not required to be symmetric.

LEMMA 1. $P(Q_i \notin \mathcal{C}_\epsilon) \leq \exp(-\epsilon^2/2\alpha^2)$.

The proof follows from Chebychev's inequality. This result allows us to summarize the level of induced perturbation for any given α . Using this lemma, we can show the following corollary.

LEMMA 2.

$$\begin{aligned} & KL(N(0, Q_j^{-1}[\Lambda E \Lambda^T + \Sigma](Q_j^{-1})^T), N(0, Q_l^{-1}[\Lambda E \Lambda^T + \Sigma](Q_l^{-1})^T)) \\ & \lesssim \left| \|Q_j^{-1}\|_F^2 - \|Q_l^{-1}\|_F^2 \right|. \end{aligned}$$

Therefore the Kullback-Leibler divergence between the marginal distributions of any two groups j and l can be bounded by $\left| \|Q_j^{-1}\|_F^2 - \|Q_l^{-1}\|_F^2 \right|$ up to some constant. We define a divergence statistic between groups j and l as $d_{jl} = \sqrt{\frac{\left| \|Q_j^{-1}\|_F^2 - \|Q_l^{-1}\|_F^2 \right|}{p^2}}$. This generates a divergence matrix $D = (\{d_{jl}\})$, where larger d_{jl} imply a greater difference between the two groups.

In our multi-group model, there is no computational complication regarding specification of the ranks of the shared and individual spaces unlike other methods. We can directly rely on current methods for accommodating unknown number of factors in the single group setting (Bhattacharya and Dunson, 2011). Due to heteroscedastic latent factors, we can directly use the posterior samples of the loading matrices without applying any factor rotation. Also, computationally our method is faster than other multi-group factor models such as BMSFA due to smaller number of parameters, and better identifiability, leading to better mixing of Markov chain Monte Carlo (MCMC).

2.1.2. Tuning the parameter α for multi-group data. The hyper-parameter α controls the level of perturbation across groups. In Section 5, we show that properly tuning α is necessary to obtain accurate estimates of the loading matrix Λ . We propose a cross validation technique to choose the optimal α based on one 50-50 split. We randomly divide each group 50/50 into training and test sets. Then for a range of α values, we fit the model on the training data, and calculate the predictive log-likelihood of the test set. After integrating out the latent factors, the predictive distribution is $Q_j Y_{ij} \sim N(0, \Lambda E \Lambda^T + \Sigma)$. If there are multiple values of α with similar predictive log-likelihoods, then the smallest α is chosen.

Alternatively, we can take a fully Bayesian approach and put a prior on α . We call this method Fully Bayesian Perturbed Factor Analysis (FBPFA). We see that FBPFA performs similarly to PFA in practice, but involves a slightly more complex MCMC implementation. PFA avoids sensitivity to the prior for α but requires the computational overhead of optimal selection of α , and can potentially be less efficient in requiring a hold out sample, while also not characterizing uncertainty in estimating α .

2.2. Measurement-error model. We can modify the multi-group model to obtain improved factor estimates in single group analyses by consider-

ing observation-level perturbations. Here we observe Y_{ij} 's for $j = 1, \dots, m_i$, which are m_i many proxies of 'true' observation W_i with multiplicative measurement errors Q_{ij}^{-1} 's such that $W_i = Q_{ij}Y_{ij}$. The modified factor model is

$$(2.2) \quad \begin{aligned} Q_{ij}Y_{ij} &= \Lambda\eta_i + \epsilon_{ij}, & \epsilon_{ij} &\sim \text{MVN}(0, \Sigma), \\ Q_{ij} &\sim \text{MN}_{p \times p}(I_p, U, V) & \eta_i &\sim \text{MVN}(0, E). \end{aligned}$$

In this model, the Q_{ij} 's apply a multiplicative perturbation to each data vector. We have $Y_{ij} = Q_{ij}^{-1}W_i$ where Q_{ij}^{-1} is a matrix. Thus, here the measurement errors are $U_{ij} = (Q_{ij}^{-1} - I_p)W_i$ and $E(U_{ij}|W_i) = 0$. This model is different from the multiplicative measurement error model of [Sarkar et al. \(2018\)](#). In their paper, observations Y_{ij} 's are modeled as $Y_{ij} = W_i \circ U_{ij}$, where \circ denotes the element wise dot product and U_{ij} 's are independent of W_i with $E(U_{ij}) = 1$. Thus, the measurement error in the l -th component (i.e. U_{ijl}) is dependent on W_i primarily through W_{il} . However, in our construction, it depends on the entire vector W_i . Thus, the measurement errors are a linear function of the entire true observation W_i .

This is a much more general setup than [Sarkar et al. \(2018\)](#). With this generality comes issues in identifying parameters in the distributions of Q_{ij} and Y_{ij} . For simplicity, we again assume $U = V = \alpha I_p$. In this case we have,

$$\begin{aligned} E(Q_{ij}Y_{ij}) &= 0 \\ V(Q_{ij}Y_{ij}) &= E(V(Q_{ij}Y_{ij}|Q_{ij})) + V(E(Q_{ij}Y_{ij}|Q_{ij})) \\ &= E(V(Q_{ij}Y_{ij}|Q_{ij})) + 0 = \alpha^2 s I_p + H, \quad s = \sum_{j=1}^p H_{jj} \end{aligned}$$

Thus, only the diagonal elements of H are not identifiable and the perturbation parameter α does not influence the dependence structure among the variables. Hence, with our heteroscedastic latent factors, we can still recover the loading structure. To tune α , we can use the marginal distributions $Q_{ij}Y_{ij} \sim \text{MVN}(0, \alpha^2 s I_p + H)$ to develop a cross validation technique when $m_i > 1$ for all $i = 1, \dots, n$ as in [Section 2.1.2](#). We split the data into training and testing sets. Then fit the model in the training set and find the α minimizing predictive log-likelihood in the test set. We can alternatively estimate α as in FBPFA by using a weakly informative prior concentrated on small values, while assessing sensitivity to hyperparameter choice.

2.3. The special case $Q_j = I_p$ for all j . For a single study dataset without any measurement error, we can modify our PFA method by taking

$Q_j = I_p$ for all j . Then the model reduces to a traditional factor model with heteroscedastic latent factors:

$$(2.3) \quad \begin{aligned} Y_i &= \Lambda \eta_i + \epsilon_i, & \epsilon_i &\sim N(0, \Sigma) \\ \eta_i &\sim \text{MVN}(0, E), \end{aligned}$$

where E is assumed to be diagonal with non-identical entries. Integrating out the latent factors, the marginal likelihood is $Y_i \sim \text{MVN}(0, \Lambda E \Lambda^T + \Sigma)$. Except for the diagonal matrix E , the marginal likelihood is similar to the marginal likelihood for a traditional factor model. As E has non-identical diagonal entries, the likelihood is no longer invariant under arbitrary rotations. For the factor model in (1.1), (Λ, η) and $(\Lambda R, R^T \eta)$ have equivalent likelihoods for any orthonormal matrix R . This is not the case in our model unless R is a permutation matrix. Thus, this simple modification over the traditional factor model helps to efficiently recover the true loading structure. This is demonstrated in Case 1 of Section 5. We also show that the posterior is weakly consistent in the supplementary materials.

3. Prior Specification. As in [Bhattacharya and Dunson \(2011\)](#), we put the following prior on Λ to allow for automatic selection of rank and easy posterior computation:

$$\begin{aligned} \lambda_{lk} | \phi_{lk}, \tau_k &\sim N(0, \phi_{lk}^{-1} \tau_k^{-1}), \\ \phi_{lk} &\sim \text{Gamma}(\nu_1, \nu_1), & \tau_k &= \prod_{i=1}^k \delta_i \\ \delta_1 &\sim \text{Gamma}(\kappa_1, 1), & \delta_i &\sim \text{Gamma}(\kappa_2, 1). \end{aligned}$$

The parameters ϕ_{lk} control local shrinkage of the elements in Λ , whereas τ_k controls column shrinkage of the k -th column. For large κ_2 , we have τ_k stochastically increasing with k , which imposes greater shrinkage for columns with higher column index. The choice $\kappa_1 = 2.1$ and $\kappa_2 = 3.1$ works well in all of our simulation settings. Note that $\kappa_2 > 1$ does not always ensure cumulative shrinkage [Durante \(2017\)](#).

For the heteroscedastic latent factors, each diagonal element of E has an independent prior:

$$e_i \sim \text{IG}(d, 0.1)$$

for some constant d . In our simulations, we see that d has minimal influence on the predictive performance of PFA. However, as d increases, more shrinkage is placed on the latent factors. We choose $d = 10$ for most of our

simulations. For the residual error variance Σ , we place a weakly informative prior on the diagonal elements:

$$\sigma_i \sim \text{IG}(0.1, 0.1).$$

In our simulations, a weakly informative $\text{IG}(0.1, 0.1)$ prior on α works well in terms of both predictive performance and estimation of the loading structure, including in single group analyses.

4. Computation. Posterior inference is straightforward with a Gibbs sampler, because all of the parameters have conjugate full conditional distributions. For the model in (2.1), the full conditional of the perturbation matrix Q_j is:

$$\text{vec}(Q_j)|Y \sim \text{MVN}(\Gamma_j(V \otimes U)^{-1}\text{vec}(I_p), \Gamma_j),$$

where $\Gamma_j = [(V \otimes U)^{-1} + S_j \otimes H^{-1}]^{-1}$ and $S_j = \sum_i Y_{ij} Y_{ij}^T$. The notation \otimes stands for Kronecker's product. The full conditionals for all other parameters are described in [Bhattacharya and Dunson \(2011\)](#), replacing Y_{ij} by $Q_j Y_{ij}$. For the model in (2.2), the full conditional of Q_{ij} is:

$$\text{vec}(Q_{ij})|Y \sim \text{MVN}(\Gamma_{ij}(V \otimes U)^{-1}\text{vec}(I_p), \Gamma_{ij}),$$

where $\Gamma_{ij} = [(V \otimes U)^{-1} + S_{ij} \otimes H^{-1}]^{-1}$ and $S_j = Y_{ij} Y_{ij}^T$. Other parameters can again be updated using the results in [Bhattacharya and Dunson \(2011\)](#) replacing Y_{ij} by $Q_{ij} Y_{ij}$. To sample the entire $\text{vec}(Q_{ij})$ or $\text{vec}(Q_j)$ together, we need to invert a $p^2 \times p^2$ matrix at each step. Instead we iteratively update the columns of Q_{ij} or Q_j , which does not require matrix inversion when $U = V = \alpha I_p$. For simplicity in notation, we only show the update for the columns in Q_j of the model in (2.1). The full conditional of the l -th column in Q_j is

$$Q_{j,l}|Y \sim \text{N}(M_l V_l, V_l),$$

where $V = 1/(\sum_{k \in G_j} Y_{l,k}^2 / \text{diag}(\Sigma) + 1/\alpha)$ and $M_l = -\sum_{k \in G_j} (Q_{j,-l} Y_{-l,k} - \Lambda \eta_k) Y_{l,k} / \Sigma + g_l / \alpha$, with Σ the diagonal error covariance matrix. Here $Q_{j,-l}$ denotes the $p \times (p-1)$ dimensional matrix removing the l -th column from Q_j . Similarly $Y_{-l,k}$ denotes the response of the k -th individual from group G_j , removing the l -th variable, and g_l the p -dimensional vector with one in the l -th entry. If we put a prior on α , the posterior distribution of α is given by $\text{IG}(0.1 + (J-1)p^2, 0.1 + \sum_j \|Q_j - I_p\|_F^2)$ for the model in (2.1) and for the model in (2.2), the posterior distribution of α is $\text{IG}(0.1 + p^2 \sum_i m_i, 0.1 + \sum_{ij} \|Q_{ij} - I_p\|_F^2)$. The posterior distribution of σ_{1l}^2 is $\text{IG}(0.1 + n/2, 0.1 + \sum_{j=1}^J \sum_{k \in G_j} (Q_j(l, \cdot) Y_{kj} - \lambda_l \eta_{kj})^2 / 2)$, where $Q_j(l, \cdot)$ denotes the l -th row of Q_j . The posterior distribution of σ_{2l}^2 is $\text{IG}(0.1 + n/2, 0.1 + \sum_{j=1}^J \sum_{k \in G_j} \eta_{l,kj}^2 / 2)$.

5. Simulation Study. In this section, we study the performance of our method in various simulation settings. As ground truth, we consider the two loading matrices given in Figure 3. These are similar to ones considered in Ročková and George (2016). R code to generate these matrices is provided in the the supplementary materials. The two matrices both have 5 columns, the first has 21 rows, and the second has 128 rows. We compare the estimated loading matrices for different choices of hyperparameters. We investigate the perturbation parameter α and the shape parameter d , which controls the level of shrinkage on the diagonal entries of E . We use the `mat2cols()` function from Murphy et al. (2018) to plot the loading matrices.

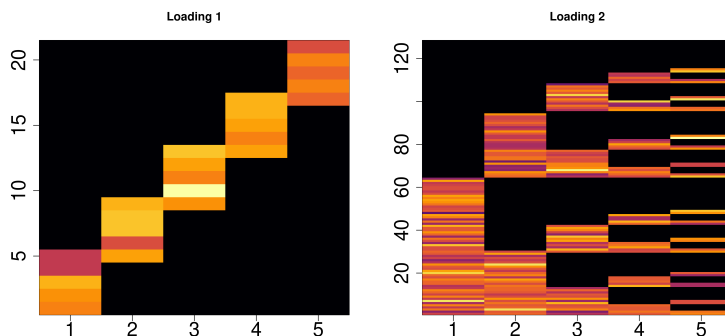


FIG 3. The ground truth loading matrices of dimension 21×5 (Loading 1) and 128×5 (Loading 2) respectively.

For the single group case, we compare with the method of Bhattacharya and Dunson (2011) (B&D), which corresponds to the spacial case of our approach that fixes the perturbation matrices and latent factor covariances equal to the identity. A point estimate of the loading matrix for B&D is calculated by post-processing the posterior samples. We use the algorithm of Afmann, Boysen-Hogrefe and Pape (2016) to rotationally align the samples of Λ , as in De Vito et al. (2018). In contrast, our method does not require any post-processing. We simply take the mean of the posterior samples to estimate the loading matrix. For the multi-group case, we compare our estimates with Bayesian Multi-Study Factor Analysis (BMSFA), which also requires post-processing to remove rotational ambiguity. We use the MSFA package from <https://github.com/rdevito/MSFA>.

We compare the different methods using predictive log likelihood. Simulated data are randomly divided 50/50 into training and test sets. After fitting each model on the training data, we calculate the predictive log like-

likelihood of the test set. All methods are run for 7000 iterations of the Gibbs sampler, with 2000 burn-in samples. Each simulation is replicated 30 times.

5.1. *Case 1: Single group, $Q_j = I_p$.* We first consider single group factor analysis. Starting with the two loading matrices in Figure 3, we simulate latent factors from $MVN(0, I_5)$, and generate datasets of 500 observations, with residual variance $\Sigma = I_5$. We compare B&D with our method when $Q_j = I_5$, so the only adjustment is to use heteroscedastic latent factors. Note that the simulated latent factors actually have identical variances.

In Tables 3 and 4, we compare methods by MSE of the estimated versus true covariance matrix. For loading matrix 1, Bayesian FA had an MSE of 2.59, which is dominated by our method across a range of values of d .

TABLE 3
MSE of estimated covariance matrix for loading matrix 1, across different values of d

d	MSE
0.1	1.04
10	1.32
100	1.38

For loading matrix 2, Bayesian FA had a MSE of 10.81. Again, our method beats this across a range of values of d . The B&D model is a special case of PFA with $E = I_p$ in (2.3). We conjecture that the gains seen for PFA are due to the more flexible induced shrinkage structure on the covariance matrix.

TABLE 4
MSE of estimated covariance matrix for loading matrix 2, across different values of d

d	MSE
0.1	5.21
10	9.45
100	10.32

We compare the estimated and true loading matrices in Figure 4. Our method performs overwhelmingly better at estimating the true loading structure compared with B&D FA. The first five columns of the estimated loadings based on our method are very close to the true loading structure under some permutation. This gain over B&D may be due to a combination of the more flexible shrinkage structure and the avoidance of the need for post-processing. We do see sensitivity to the hyperparameter d , which is as expected. Estimation MSE is better for smaller d , but the general structure of the loadings matrix is recovered accurately for all d .

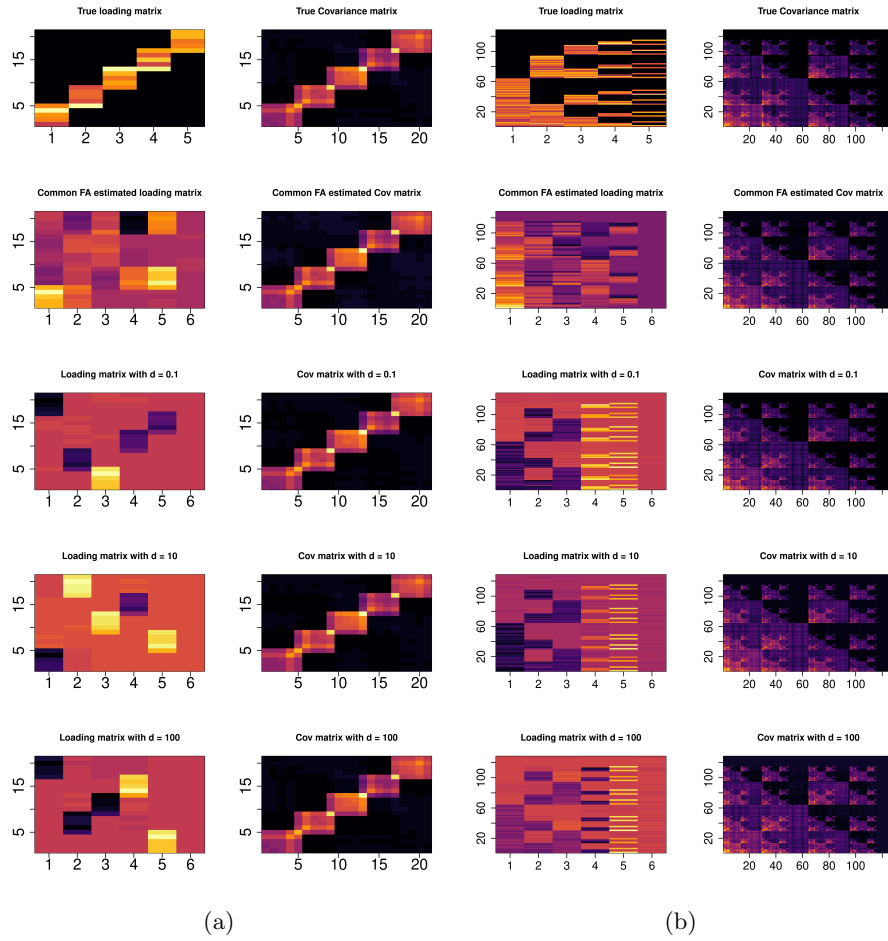


FIG 4. Comparison of true and estimated loading matrices and covariance matrices for case 1. Comparison of $B^{\mathcal{E}D}$ FA with our method for different choices of d . Results for loading matrix 1 are in (a) and 2 in (b). For all the cases, we fix $Q_j = I$.

5.2. *Case 2: Multi-group, multiplicative perturbation.* In this case, we simulate data from the multi-group model in (2.1) for $i = 1, \dots, 500$. Observations Y_i are first generated using the same method as in case 1. The data are then split into 10 groups of 50 observations, such that $G_j = \{Y_k : 50(j-1) \leq k \leq 50j\}$ for $j = 1, \dots, 10$. The groups are perturbed using matrices $Q_{j0} \sim \text{MN}(I_p, \alpha_0 I_p, \alpha_0 I_p)$ for different choices of α_0 , setting $Q_1 = I_p$.

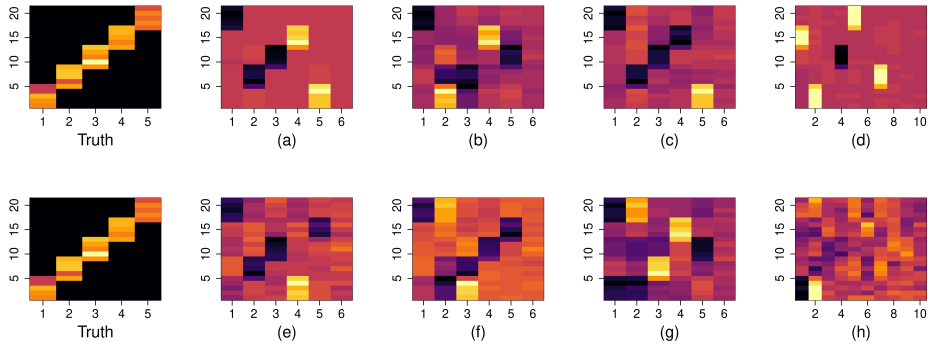


FIG 5. Comparison of estimated loading matrix 1 in simulation case 2 with different choices of α_0 and α where $Q_{j0} \sim \text{MN}(I_p, \alpha_0 I_p, \alpha_0 I_p)$ and $U = \alpha I_p = V$. (a) $\alpha = 1 \times 10^{-4}, \alpha_0 = 1 \times 10^{-4}$, (b) $\alpha = 1 \times 10^{-2}, \alpha_0 = 1 \times 10^{-4}$, (c) FBPFA with $\alpha_0 = 1 \times 10^{-4}$, (d) BMSFA with $\alpha_0 = 1 \times 10^{-4}$, (e) $\alpha = 1 \times 10^{-4}, \alpha_0 = 1 \times 10^{-2}$, (f) $\alpha = 1 \times 10^{-2}, \alpha_0 = 1 \times 10^{-2}$, (g) FBPFA with $\alpha_0 = 1 \times 10^{-2}$, (h) For BMSFA with $\alpha_0 = 1 \times 10^{-2}$. True loading matrices are plotted twice in columns 1 for easier comparison with other images.

TABLE 5
Average predictive log-likelihood for PFA with optimal α , FBPFA and BMSFA in simulation case 2.

True Loading	α_0	PFA for optimal α	FBPFA	BMSFA
Loading 1	1×10^{-4}	-31.65	-25.92	-679.36
	1×10^{-2}	-30.32	-26.01	-921.76
Loading 2	1×10^{-4}	-210.43	-251.13	-6871.38
	1×10^{-2}	-351.42	-304.10	-25018.50

Figures 5 and 6 show the estimated loading matrices. We obtain accurate estimates even when allowing for a higher level of perturbation than the truth, $\alpha_0 \leq \alpha$. However, the estimates are best when $\alpha = \alpha_0 = 1 \times 10^{-4}$. Performance degrades more sharply when we underestimate the level of perturbation, as in the case where $\alpha = 1 \times 10^{-4}, \alpha_0 = 1 \times 10^{-2}$. The estimated loadings from PFA and FBPFA are better than BMSFA. Except for cases with higher level of perturbation using BMSFA, the estimated loadings matrix is close to the truth under some permutation of the columns. In our

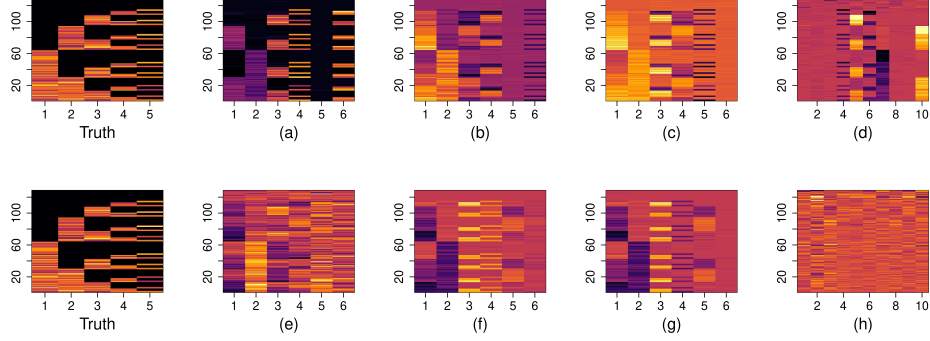


FIG 6. Comparison of estimated loading for loading matrix 2 in simulation case 2 with different choices of α_0 and α where $Q_{j_0} \sim MN(I_p, \alpha_0 I_p, \alpha_0 I_p)$ and $U = \alpha I_p = V$. (a) $\alpha = 1 \times 10^{-4}, \alpha_0 = 1 \times 10^{-4}$, (b) $\alpha = 1 \times 10^{-2}, \alpha_0 = 1 \times 10^{-4}$, (c) FBPFA with $\alpha_0 = 1 \times 10^{-4}$, (d) BMSFA with $\alpha_0 = 1 \times 10^{-4}$, (e) $\alpha = 1 \times 10^{-4}, \alpha_0 = 1 \times 10^{-2}$, (f) $\alpha = 1 \times 10^{-2}, \alpha_0 = 1 \times 10^{-2}$, (g) FBPFA with $\alpha_0 = 1 \times 10^{-2}$, (h) BMSFA with $\alpha_0 = 1 \times 10^{-2}$. True loading matrices are plotted twice in columns 1 for easier comparison with other images.

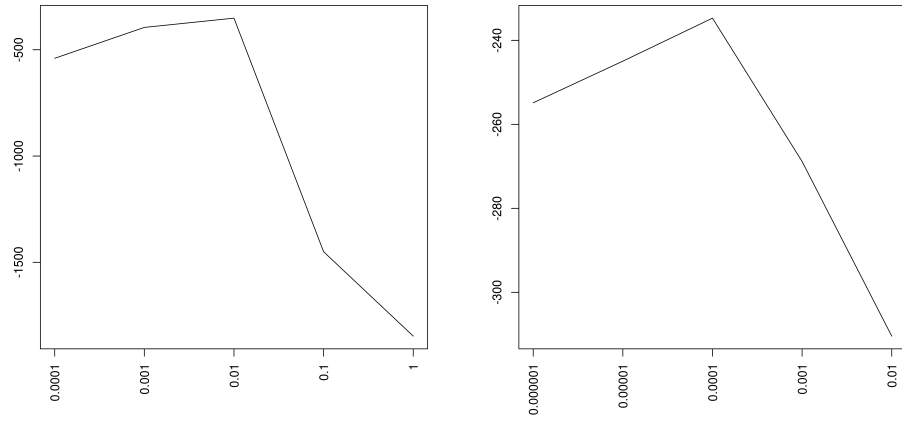


FIG 7. Average predictive log-likelihoods for different choices of α in simulation case 2 for two cases - in the first case the perturbation matrices are generated using true $\alpha_0 = 1 \times 10^{-2}$ and in the second case $\alpha_0 = 1 \times 10^{-4}$. This is based on the simulation experiment of Figure 6. Uncertainties in estimation of predictive log-likelihoods are included as labels on the top of each point.

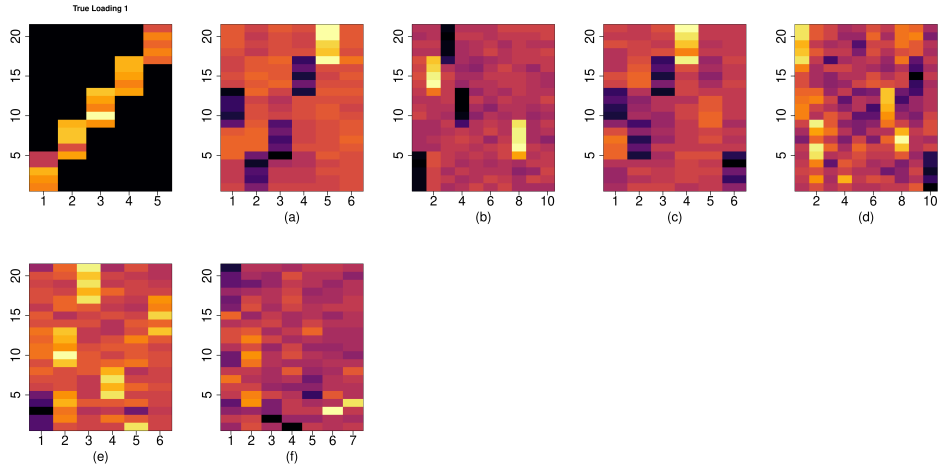


FIG 8. Comparison of estimated loading matrices in simulation case 2 with increasing error variances and $\alpha_0 = 1 \times 10^{-4}$: (a) $\alpha = 1 \times 10^{-4}$ with error variance 25, (b) $\alpha = 1 \times 10^{-4}$ with error variance 100, (c) BMSFA with error variance 25, (d) BMSFA with error variance 100, (e) FBPFA with error variance 25, (f) FBPFA with error variance 100.

method, considering only the first five columns of the estimated loadings is sufficient to accurately estimate the loading structure. All the other columns can be removed due to their very small contribution. We also apply the same simulation setting with higher error variances. Figure 8 compares the estimated loadings. All the methods identify the true structure when the residual standard deviation is 5, but only PFA with correctly specified α produces good estimates when we increase it to 10.

In Figure 7, we show the predictive likelihood under a range of α values. For each choice of α on the x axis, we fit the model to a training set and calculate the predictive log-likelihood on a test set. These are plotted on the y-axis. This demonstrates the utility of our cross-validation technique in finding the optimal α . In Table 5, we compare the performance of PFA with optimal α , FBPFA and BMSFA in terms of predictive likelihood. PFA and FBPFA have overwhelmingly better performance. We also calculate the uncertainty of the predictive log-likelihood for each choice of α . For both of the two cases in Figure 7, the uncertainty increases as we increase α .

5.2.1. *Case 2.1: Partially shared factors.* We also repeat the case 2 simulation but modified to accommodate a partially shared structure. In particular, we generated the data as in case 2 but for the last two groups we let $Q_j Y_i \sim \text{MVN}(\Lambda_{01} \Lambda_{01}^T + I_p)$ for $i \in G_j$ and $j = 9, 10$. Here $\Lambda_{01} = \Lambda_0[1 : 3]$ is

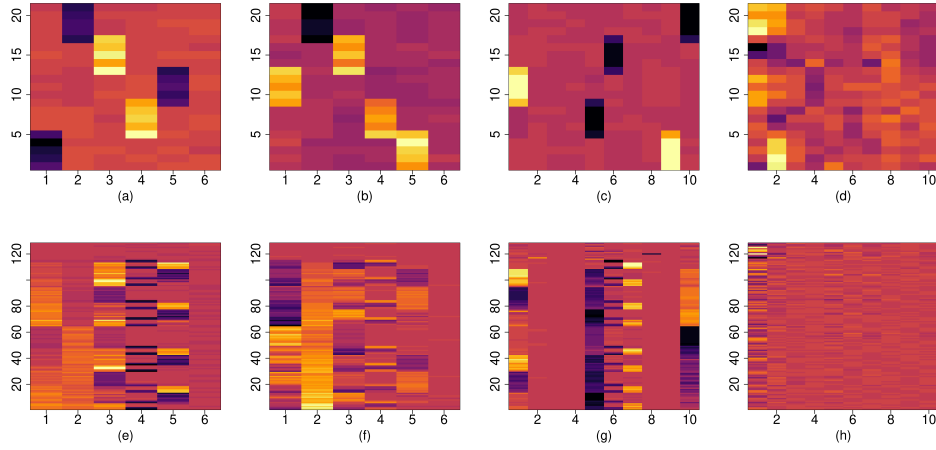


FIG 9. Comparison of estimated loading in the partially shared modification of simulation case 2. Row 1 corresponds to true loading structure 1 and row 2 to true loading structure 2. (a) FBPFA with $\alpha_0 = 1 \times 10^{-4}$, (b) FBPFA with $\alpha_0 = 1 \times 10^{-2}$, (c) BMSFA with $\alpha_0 = 1 \times 10^{-4}$, (d) BMSFA with $\alpha_0 = 1 \times 10^{-2}$, (e) FBPFA with $\alpha_0 = 1 \times 10^{-4}$, (f) FBPFA with $\alpha_0 = 1 \times 10^{-2}$, (g) BMSFA with $\alpha_0 = 1 \times 10^{-4}$, (h) BMSFA with $\alpha_0 = 1 \times 10^{-2}$.

$p \times 3$ dimensional matrix having the first three columns from Λ_0 . The choices for Λ_0 are given in Figure 3. The estimated loading matrices are compared in Figure 9 for two levels of perturbations, $\alpha_0 = 1 \times 10^{-4}, 1 \times 10^{-2}$, and two different true loadings matrices. FBPFA works well for any level of perturbation, while BMSFA works well for only the lower perturbation level.

5.3. *Case 3: Multi-group factor model.* In this case, we generate data from the Bayesian multi-study factor analysis (BMSFA) model as in De Vito et al. (2018).

$$(5.1) \quad \begin{aligned} Y_i &= \Lambda \eta_{i1} + \Psi_j \eta_{i2} + \epsilon_{1i} \text{ and } Y_i \in G_j, \\ \epsilon_{1i} &\sim \text{MVN}(0, \Sigma) \quad \eta_{i1}, \eta_{i2} \sim N(0, I_p), \end{aligned}$$

where the group specific loadings (Ψ_j 's) are lower in magnitude in comparison to the shared loading matrix Λ . It is expected that as the magnitude in group specific loading increases, the estimation of the share loading becomes increasingly difficult. This motivates us to consider two types of Ψ_j 's. First we generate the elements in Ψ_j from $N(-0.2, 0.2)$. Next we generate those from $N(-0.5, 0.8)$. These matrices are the same dimension as the shared loading matrix Λ . Figure 10 compares the estimated loadings with the true shared loadings across different methods PFA for two different perturbation parameter, FBPFA and BMSFA. Although we generate the data

from BMFSA, all the estimates are very much comparable in Figure 10. However, PFA and FBPFA again outperform BMSFA in terms of predictive log-likelihoods as shown in Table 6. In the the supplementary material, we present another simulation setting akin to BMSFA. There, the data generating process is similar to BMSFA with minor modifications in the shared and group-specific loading structures.

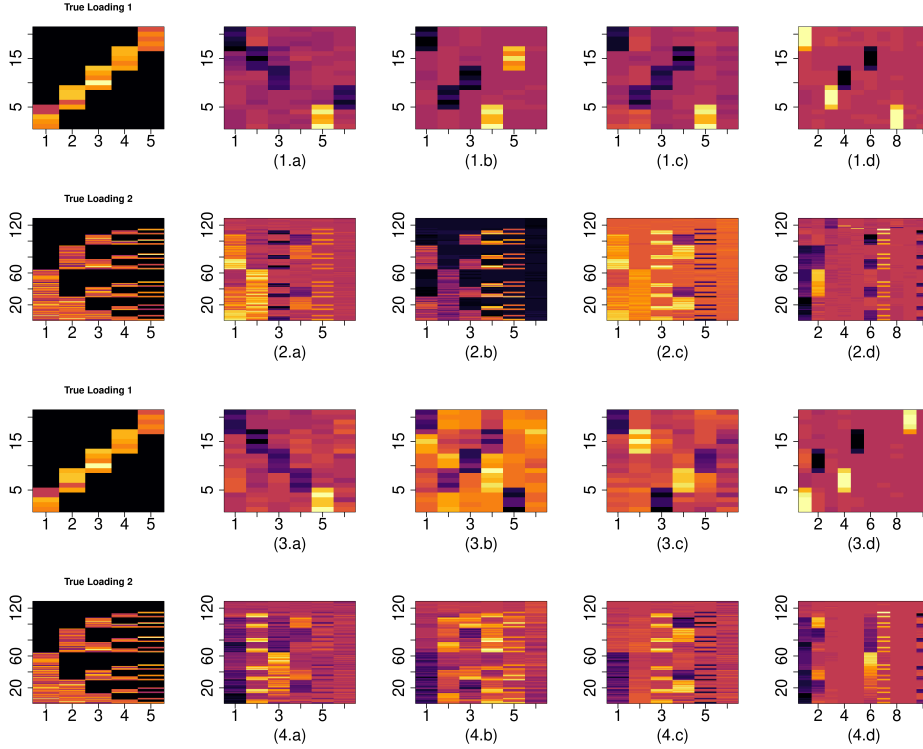


FIG 10. Comparison of estimated loading matrices in Simulation Case 3 when the true data generating process follows the model in (5.1). For the first two rows, true Ψ_j 's are generated from $N(-0.2, 0.2)$ and for the last two rows Ψ_j 's are generated from $N(-0.5, 0.8)$ and for each row (a) PFA with $\alpha = 1 \times 10^{-2}$, (b) PFA with $\alpha = 1 \times 10^{-4}$, (c) FBPFA, (d) BMSFA

5.4. *Case 4: Mimic NHANES data.* In this section, we generate the data from the model in (2.1). However, the model parameters Q_j 's and Λ are first estimated on the HHANES data with $\alpha = 1 \times 10^{-2}$. Then, based on these estimated parameters, we generate the data following the same model. Figure 11 compares the estimated loadings across all the methods, PFA for different choices of α , FBPFA and BSSFA. We find that all the methods

TABLE 6
Average predictive log-likelihood for PFA for different choices of α , FBPFA and BMSFA in Simulation Case 3.

Generative Distribution of Ψ_j 's	True Loading	PFA for $\alpha = 1 \times 10^{-2}$	PFA for $\alpha = 1 \times 10^{-4}$	FBPFA	BMSFA
N(-0.2, 0.2)	Loading 1	-33.41	-44.10	-26.16	-500.66
	Loading 2	-336.58	-259.79	-265.77	-9547.77
N(-0.5, 0.8)	Loading 1	-49.25	-53.32	-37.89	-720.35
	Loading 2	-584.82	-308.72	-1003.02	-14187.36

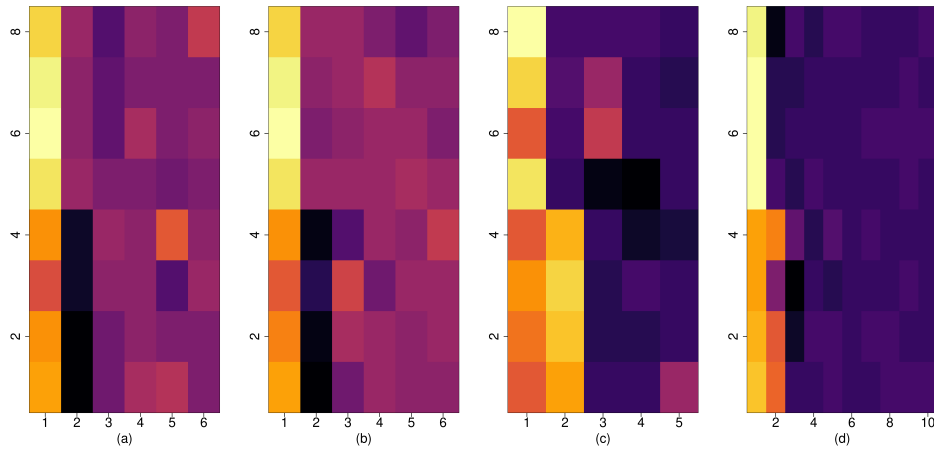


FIG 11. Comparison of estimated loading matrices in Simulation Case 4 where the true loading matrix is PFA estimated loading with $\alpha = 1 \times 10^{-2}$ for standardized NHANES data and the data is simulated from the model (2.1). (a) PFA with $\alpha = 1 \times 10^{-4}$, (b) PFA with $\alpha = 1 \times 10^{-2}$, (c) FBPFA, (d) BMSFA

recover identical loading structures which match with our estimated loadings from Section 6. Because of the truncation of columns having significantly low contributions, the PFA and FBPFA estimated loadings have smaller number of columns than BMSFA.

6. Application to NHANES data. We fit our model in (2.1) to the NHANES dataset as described in Section 2 to get a shared set of factors. In our analysis, we consider the standardized data and explore shared structures. In this standardized data, the mean chemical levels are subtracted from the data across all the groups. For our analysis, the data are randomly split, with 2/3 in each group as a training set, and 1/3 as a test set. We collect 5000 post burn MCMC samples after a burn-in of 5000 samples. The

convergence is monitored based on the predictive likelihood of the test set at each MCMC iteration. The hyper parameters are the same as those in Section 5. The predictive log-likelihood of the test data is used to tune α as described in Section 2.1.2. Based on our cross-validation technique, $\alpha = 0.01$ turns out to be optimal.

Figure 12 shows the estimated loadings using PFA, FBPFA and BMSFA. We cannot plot the loading matrices using the same color levels as the matrices are not comparable in value. However, all plots show two significant factors, with some suggestions of a third factor. We see similar across all the estimates, which provides additional support for one typical summary measure, the sum of all phthalates, based on similar loadings across phthalates in one factor. For PFA and FBPFA, all the chemicals load on the first factor, and the second factor is loaded on by the last four chemicals, namely MECPP, MEHHP, MEOHP, and MEHP. Figure 1 also suggests that these four chemicals are related to each other more than the others. This is not surprising, as MECPP, MEHHP, and MEOHP are oxidative metabolites of MEHP.

We also compare PFA and FBPFA with BMSFA in terms of predictive log-likelihood in Table 7. As observed in the simulation study, PFA and FBPFA again perform much better than BMSFA in terms of the predictive log-likelihood. Among all the methods, FBPFA performs the best. We also compare PFA, FBPFA and BMSFA in terms of prediction MSEs. For prediction within our unsupervised learning framework, we collect MCMC samples of the test data given the data and model parameters. For clarity, we describe our steps in detail here. Let \mathcal{M} denote the model and Y_M and Y_O stand for missing (test) and observed (training) set of observations. We start with some initial choices of model parameters. Next, we sample the missing observations from the conditional distribution $P(Y_M|Y_O, \mathcal{M})$. After that, we sample the model parameters from $P(\mathcal{M}|(Y_O, Y_M)) \propto P((Y_O, Y_M)|\mathcal{M})P(\mathcal{M})$. We repeat these two steps iteratively. Let \hat{Y}_M be the posterior mean of the MCMC samples of Y_M . We report the prediction MSE, which is calculated as mean square difference between Y_M and \hat{Y}_M . The prediction for PFA with $\alpha = 1 \times 10^{-4}$ and $\alpha = 1 \times 10^{-2}$ are 0.09 and 0.12 respectively. It turns out to be 0.12 for FBPFA where as the same for BMSFA turns out to be 0.87.

TABLE 7
Average predictive log-likelihood for different methods

PFA for optimal α	FBPFA	BMFA
4.12	5.02	-7.99

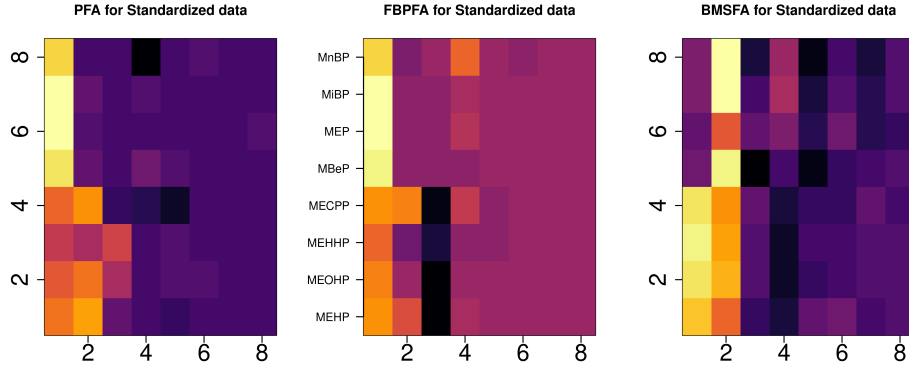


FIG 12. Comparison of estimated loading matrices with different methods. PFA estimates are based on $\alpha = 1 \times 10^{-2}$.

We calculate divergence scores and create the divergence matrix D . This is provided in Table 8 to explore similarities across groups. To summarize D , we also provide in Figure 13 a network plot between different groups. The edge-width between two nodes (j, l) is calculated as $60/d_{jl}$. Thus, the edge-width is inversely proportional to the divergence statistic. Thicker edges imply greater similarity. Hence, this figure implies that non-Hispanic whites differ the most in exposure from the other groups, supporting the findings of our exploratory ANOVA analysis in the supplementary materials and findings in the prior literature (Bloom et al., 2019). We find evidence of one extra factor among non-Hispanic whites relative to the other groups in Figure 2. The two Hispanic ethnicity groups are very similar in loadings as shown in Figure 2 and also their Hotelling T^2 distance is relatively small in Table 2. Our results based on divergence scores also suggest similar distinctions among the groups. Also these results support our preliminary analysis, described in Section 2. In Table 9, we show square norm difference between the group specific loadings, estimated using BMSFA and the associated postprocessing. The (i, j) -th entry of the table is calculated as $\sqrt{\sum_{lk} (A_{ill} - A_{jlk})^2}$, where the matrices A_i and A_j are the estimated group-specific loadings for the groups i and j respectively using BMSFA. These numbers do not suggest similar clustering of the racial groups as we can conclude using our PFA method. All the groups seem to be almost equal distance apart from each other using that approach.

7. Discussion. Our over-arching goal was to develop a less brittle method for estimating factors that hold across similar datasets and groups within a

TABLE 8
Estimated divergence scores for different pairs of groups.

	Mex	OH	N-H White	N-H Black	Other/Multi
Mex	0.00	5.86	41.35	10.22	3.82
OH	5.86	0.00	40.93	8.38	4.45
N-H White	41.35	40.93	0.00	40.06	41.17
N-H Black	10.22	8.38	40.06	0.00	9.48
Other/Multi	3.82	4.45	41.17	9.48	0.00

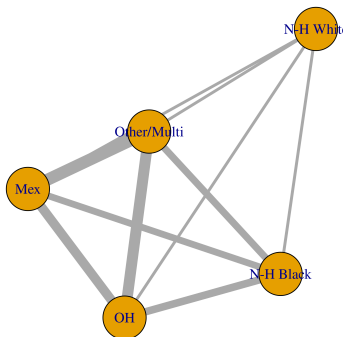


FIG 13. *Network plot summarizing similarity between the groups based on the divergence metric where thicker edge implies smaller divergence score. The group names are mentioned for each node.*

dataset. In many applications, it is important to define a more generalizable set of factors, improving on the current status in which one often obtains dramatically different factors when fitting a factor model separately to different groups or using current additive ANOVA-type factor models. A primary innovation of the article is to incorporate a multiplicative perturbation of the data. As we have shown, this can be included in many different contexts - ranging from meta analysis, to multiple group data, to measurement error modeling, and even to obtain improved performance when there is no group or replicated structure in the data. We have demonstrated exciting improvements in performance in all of these settings.

It is our hope that the proposed method can be used directly by epidemiologists, and scientists in other fields, to obtain more generalizable factors in their applications. This will be important in understanding the extent to which well-known disparities in health outcomes, such as material and child birth outcomes or obesity, may be influenced by meaningful differences in exposures to phthalate and other chemicals pervasive in our home and work environment. With this goal in mind, we have provided code for implementing the proposed approach at <https://github.com/royarkaprava/>

TABLE 9
Square norm difference of the group-specific loadings, estimated using BMSFA.

	Mex	OH	N-H White	N-H Black	Other/Multi
Mex	0.00	0.75	0.70	0.59	0.78
OH	0.75	0.00	0.63	0.75	0.73
N-H White	0.70	0.63	0.00	0.68	0.84
N-H Black	0.59	0.75	0.68	0.00	0.91
Other/Multi	0.78	0.73	0.84	0.91	0.00

Perturbed-factor-model. To make the method more broadly useful, there are a number of interesting extensions, some trivial and some less so. The first is to adjust for covariates - this can be very easily done without modifying the fundamental approach with a simple tweak to the proposed Gibbs sampler. Another important modification is to allow data that are not simply all continuous variables but may be categorical or mixed categorical and continuous. This can rely on an underlying variable model, as is often used in factor analysis (see, for example, [Carvalho et al. \(2008\)](#); [Zhou et al. \(2015\)](#)). In this case, we would incorporate the perturbation in the underlying variables instead of in the observed data directly. Again, this leads to a minor modification of the proposed Gibbs sampling algorithm.

We conjecture that both the perturbation ideas and the idea of including heterogeneous factor variances to improve identifiability will have impact beyond the specific setting we have considered in this paper. For example, one natural extension is to non-linear factor models, such as Gaussian process latent variable models ([Lawrence, 2004](#); [Lawrence and Quiñonero-Candela, 2006](#)) and variational auto-encoders ([Kingma and Welling, 2013](#); [Pu et al., 2016](#)). For simplicity, we have considered identical entries in the diagonal of U and V . This suggests homoscedastic perturbation across all the variables. However, one potential future direction is allow for different levels of perturbations across different variables. Thus one can assume $U = \text{diag}(\alpha_1, \dots, \alpha_p)$ and similarly on V . If inter-group variations are large, one possibility is to consider group specific perturbation parameters such as $Q_j \sim \text{MN}(I_p, \alpha_j I_p, \alpha_j I_p)$. Since it requires to choose optimal α_j 's simultaneously for all the groups, considering FBPFPA framework is more suitable. Thus, we can put weakly informative $\text{IG}(0.1, 0.1)$ prior of α_j . Furthermore, the shape parameter d is kept fixed at 100. In [Figure 4](#), we find that the estimates are not very sensitive to the choice of d in recovering true loading structure. However, one can put a hyper prior on d such as weakly informative $\text{IG}(0.1, 0.1)$ and make more robust inferences.

8. Acknowledgments. This research was partially supported by grant R01-ES027498 from the National Institute of Environmental Health Sciences (NIEHS) of the National Institutes of Health (NIH). We would like to thank Roberta De Vito for sharing her source code of the Bayesian MSFA model. We would also like to thank Noirrit Kiran Chandra for his feedbacks on the code which heavily improved its usage both in low and high dimensional settings.

References.

- ASSMANN, C., BOYSEN-HOGREFE, J. and PAPE, M. (2016). Bayesian analysis of static and dynamic factor models: An ex-post approach towards the rotation problem. *Journal of Econometrics* **192** 190–206.
- BENJAMIN, S., MASAI, E., KAMIMURA, N., TAKAHASHI, K., ANDERSON, R. C. and FAISAL, P. A. (2017). Phthalates impact human health: epidemiological evidences and plausible mechanism of action. *Journal of Hazardous Materials* **340** 360–383.
- BHATTACHARYA, A. and DUNSON, D. B. (2011). Sparse Bayesian infinite factor models. *Biometrika* 291–306.
- BLOOM, M. S., WENZEL, A. G., BROCK, J. W., KUCKLICK, J. R., WINELAND, R. J., CRUZE, L., UNAL, E. R., YUCEL, R. M., JIYESSOVA, A. and NEWMAN, R. B. (2019). Racial disparity in maternal phthalates exposure; Association with racial disparity in fetal growth and birth outcomes. *Environment International* **127** 473–486.
- CARVALHO, C. M., CHANG, J., LUCAS, J. E., NEVINS, J. R., WANG, Q. and WEST, M. (2008). High-dimensional sparse factor modeling: applications in gene expression genomics. *Journal of the American Statistical Association* **103** 1438–1456.
- DE VITO, R., BELLIO, R., TRIPPA, L. and PARMIGIANI, G. (2018). Bayesian Multi-study Factor Analysis for High-throughput Biological Data. *arXiv preprint arXiv:1806.09896*.
- DE VITO, R., BELLIO, R., TRIPPA, L. and PARMIGIANI, G. (2019). Multi-study factor analysis. *Biometrics* **75** 337–346.
- DURANTE, D. (2017). A note on the multiplicative gamma process. *Statistics & Probability Letters* **122** 198–204.
- FENG, Q., HANNIG, J. and MARRON, J. (2015). Non-iterative joint and individual variation explained. *arXiv preprint arXiv:1512.04060*.
- FENG, Q., JIANG, M., HANNIG, J. and MARRON, J. (2018). Angle-based joint and individual variation explained. *Journal of Multivariate Analysis* **166** 241–265.
- FRUEHWIRTH-SCHNATTER, S. and LOPES, H. F. (2018). Sparse Bayesian Factor Analysis when the Number of Factors is Unknown. *arXiv preprint arXiv:1804.04231*.
- JAMES-TODD, T. M., MEEKER, J. D., HUANG, T., HAUSER, R., SEELY, E. W., FERGUSON, K. K., RICH-EDWARDS, J. W. and McELRATH, T. F. (2017). Racial and ethnic variations in phthalate metabolite concentration changes across full-term pregnancies. *Journal of Exposure Science and Environmental Epidemiology* **27** 160.
- KIM, S. H. and PARK, M. J. (2014). Phthalate exposure and childhood obesity. *Annals of Pediatric Endocrinology & Metabolism* **19** 69.
- KIM, S., KANG, D., HUO, Z., PARK, Y. and TSENG, G. C. (2018). Meta-analytic principal component analysis in integrative omics application. *Bioinformatics* **34** 1321–1328.
- KINGMA, D. P. and WELING, M. (2013). Auto-encoding variational bayes. *arXiv preprint arXiv:1312.6114*.
- LAWRENCE, N. D. (2004). Gaussian process latent variable models for visualisation of high dimensional data. In *Advances in neural information processing systems* 329–336.

- LAWRENCE, N. D. and QUIÑONERO-CANDELA, J. (2006). Local distance preservation in the GP-LVM through back constraints. In *Proceedings of the 23rd international conference on Machine learning* 513–520. ACM.
- LEE, S. X., LIN, T.-I. and MCLACHLAN, G. J. (2018). Mixtures of factor analyzers with fundamental skew symmetric distributions. *arXiv preprint arXiv:1802.02467*.
- LOCK, E. F., HOADLEY, K. A., MARRON, J. S. and NOBEL, A. B. (2013). Joint and individual variation explained (JIVE) for integrated analysis of multiple data types. *The Annals of Applied Statistics* **7** 523.
- LOPES, H. F. and WEST, M. (2004). Bayesian model assessment in factor analysis. *Statistica Sinica* 41–67.
- MARESCA, M. M., HOEPNER, L. A., HASSOUN, A., OBERFIELD, S. E., MOONEY, S. J., CALAFAT, A. M., RAMIREZ, J., FREYER, G., PERERA, F. P., WHYATT, R. M. et al. (2016). Prenatal exposure to phthalates and childhood body size in an urban cohort. *Environmental Health Perspectives* **124** 514–520.
- MCPARLAND, D., GORMLEY, I. C., MCCORMICK, T. H., CLARK, S. J., KABUDULA, C. W. and COLLINSON, M. A. (2014). Clustering South African households based on their asset status using latent variable models. *The Annals of Applied Statistics* **8** 747.
- MURPHY, K., VIROLI, C., GORMLEY, I. C. et al. (2018). Infinite mixtures of infinite factor analysers. *Bayesian Analysis*.
- PU, Y., GAN, Z., HENAO, R., YUAN, X., LI, C., STEVENS, A. and CARIN, L. (2016). Variational autoencoder for deep learning of images, labels and captions. In *Advances in neural information processing systems* 2352–2360.
- ROČKOVÁ, V. and GEORGE, E. I. (2016). Fast Bayesian factor analysis via automatic rotations to sparsity. *Journal of the American Statistical Association* **111** 1608–1622.
- ROY, A., SCHAICH-BORG, J. and DUNSON, D. B. (2019). Bayesian time-aligned factor analysis of paired multivariate time series. *arXiv preprint arXiv:1904.12103*.
- SARKAR, A., PATI, D., CHAKRABORTY, A., MALLICK, B. K. and CARROLL, R. J. (2018). Bayesian semiparametric multivariate density deconvolution. *Journal of the American Statistical Association* **113** 401–416.
- SCHWARTZ, L. (1965). On bayes procedures. *Zeitschrift für Wahrscheinlichkeitstheorie und verwandte Gebiete* **4** 10–26.
- SEBER, G. A. (2009). *Multivariate observations* **252**. John Wiley & Sons.
- TAYLOR, K. W., TROESTER, M. A., HERRING, A. H., ENGEL, L. S., NICHOLS, H. B., SANDLER, D. P. and BAIRD, D. D. (2018). Associations between personal care product use patterns and breast cancer risk among white and black women in the sister study. *Environmental health perspectives* **126** 027011.
- WEISSENBURGER-MOSER, L., MEZA, J., YU, F., SHIYANBOLA, O., ROMBERGER, D. J. and LEVAN, T. D. (2017). A principal factor analysis to characterize agricultural exposures among Nebraska veterans. *Journal of Exposure Science and Environmental Epidemiology* **27** 214.
- ZHANG, Y., MENG, X., CHEN, L., LI, D., ZHAO, L., ZHAO, Y., LI, L. and SHI, H. (2014). Age and sex-specific relationships between phthalate exposures and obesity in Chinese children at puberty. *PloS one* **9** e104852.
- ZHOU, J., BHATTACHARYA, A., HERRING, A. H. and DUNSON, D. B. (2015). Bayesian factorizations of big sparse tensors. *Journal of the American Statistical Association* **110** 1562–1576.

9. Supplementary.

9.1. *Posterior consistency.* Let $\Theta_\Lambda, \Theta_\Sigma, \Theta_E$ be the parameter spaces of Λ, Σ and E , respectively, Θ be the set of $p \times p$ positive semidefinite matrices corresponding to the parameter space of H , and \mathcal{Q}_j be the parameter space of Q_j . Let $\Pi_\Lambda, \Pi_\Sigma, \Pi_E, \Pi_Q$ be the priors for Λ, Σ, E and Q_j 's. We restate some of the results from [Bhattacharya and Dunson \(2011\)](#) for our modified factor model. With minor modification, the proofs will remain the same.

Let $g : \Theta_\Lambda \times \Theta_\Sigma \times \Theta_E \rightarrow \Theta_H$ be a continuous map such that $g(\Lambda, \Sigma, E) = \Lambda^T E \Lambda + \Sigma$.

LEMMA 3. *For any $(\Lambda, \Sigma, E) \in \Theta_\Lambda \times \Theta_\Sigma \times \Theta_E$, we have $g(\Lambda, \Sigma, E) \in \Theta_H$.*

The proof is similar to Lemma 1 of [Bhattacharya and Dunson \(2011\)](#). In our Bayesian approach, we choose independent priors for Λ, Σ and E and that induces a prior on H through the map g . We also have following proposition.

PROPOSITION 4. *If $(\Lambda, \Sigma, E) \sim \Pi_\Lambda \otimes \Pi_\Sigma \otimes \Pi_E$, then $\Pi_\Lambda \otimes \Pi_\Sigma \otimes \Pi_E(\Theta_\Lambda \times \Theta_\Sigma \times \Theta_E) = 1$.*

The proof is similar to Proposition 1 of [Bhattacharya and Dunson \(2011\)](#) with minor modifications. Now, we proceed to establish that the posterior of our multigroup model is weakly consistent under a fixed p and increasing n regime. Let us assume that the complete parameter space is $\kappa = (\Lambda, \Sigma, E, Q_2, \dots, Q_j)$ and let κ_0 be the truth for κ .

Assumptions:

1. For some $M > 0$, the true perturbation matrices are $Q_{j0} \in \mathcal{C}_M$, with \mathcal{C}_M defined in Section 2.1.1.
2. There exists some $E > 0, F_1 > 0$ and $F_2 > 0$ such that $\max_{ij} |\Lambda_0| < E$ and $F_1 < e_{0k} < F_2$ for all $k = 1, \dots, r$.

THEOREM 5. *Under Assumptions 1-2, the posterior for κ is weakly consistent at κ_0 .*

We first show that our proposed prior has large support in the sense that the truth belongs to the Kullback-Leibler support of the prior. Thus the posterior probability of any neighbourhood around the truth converges to one in $P_{\kappa_0}^{(n)}$ -probability as n goes to ∞ as a consequence of [Schwartz \(1965\)](#). Here $P_{\kappa}^{(n)}$ is the distribution of a sample of n observations with parameter κ . Hence, the posterior is weakly consistent.

PROOF. For $q, q^* \in$ the space of probability measure \mathcal{P} , let the Kullback-Leibler divergences be given by

$$KL(q^*, q) = \int q^* \log \frac{q^*}{q}.$$

Let $K(\kappa_0, \kappa)$ denote the Kullback-Leibler divergence

$$\sum_{j=1}^J KL(N(0, Q_j^{-1}[\Lambda E \Lambda^T + \Sigma](Q_j^T)^{-1}), N(0, Q_{j0}^{-1}[\Lambda_0 E_0 \Lambda_0^T + \Sigma_0](Q_{j0}^{-1})^T)).$$

For our model, we have

$$K(\kappa_0, \kappa) = \frac{1}{2n} \left[\sum_{j=1}^J -n_j \log |Q_{j0}^{-1} H_0(Q_{j0}^T)^{-1} \{Q_j^{-1} H(Q_j^T)^{-1}\}^{-1}| \right. \\ \left. + n_j \text{tr}(Q_{j0}^{-1} H_0(Q_{j0}^T)^{-1} \{Q_j^{-1} H(Q_j^T)^{-1}\}^{-1} - I_p) \right]$$

To prove Theorem 5, we rely on the following Lemma.

LEMMA 6. *For any $\epsilon > 0$, there exists $\epsilon_1 > 0, \epsilon_2 > 0$, and $\epsilon_{3j} > 0$ for $j \in \{2, \dots, J\}$ such that $\|\Lambda - \Lambda_0\|_F^2 \leq \epsilon_1^2$, $\|E - E_0\|_F^2 \leq \epsilon_2^2$ and $\|Q_j - Q_{j0}\|_F^2 \leq \epsilon_{3j}^2$, then we have*

$$\Pi\{K(\kappa_0, \kappa) \leq \epsilon\} \geq \Pi\{\|\Lambda - \Lambda_0\|_F^2 \leq \epsilon_1^2, \|E - E_0\|_F^2 \leq \epsilon_2^2, \|Q_j - Q_{j0}\|_F^2 \leq \epsilon_{3j}^2, j = 2, \dots, J\}$$

Due to continuity of the functions such as determinant, trace and $g(\cdot)$, the above result is immediate following the proof of Theorem 2 in [Bhattacharya and Dunson \(2011\)](#). For our proposed priors, the prior probability of the R.H.S. of Lemma 6 is positive. Thus the prior probability of any Kullback-Leibler neighborhood around the truth is positive. This proves Theorem 5. \square

9.2. Additional simulations.

9.2.1. *S. Case 1: Multi-group, additive perturbation.* In Case 2, each group is multiplied by a unique perturbation matrix Q_j . In this case, we perturb the data by adding a group specific loading matrix Ψ_j to a shared loading matrix Λ , as in model (9.1).

$$(9.1) \quad \begin{aligned} Y_i &= (\Lambda + \Psi_j)\eta_i + \epsilon_{1i} \text{ and } Y_i \in G_j, \\ \epsilon_{1i} &\sim \text{MVN}(0, \Sigma) \quad \eta_i \sim N(0, I_p), \end{aligned}$$

where the group specific loadings (Ψ_j 's) are lower in magnitude in comparison to the shared loading matrix Λ . This can also be an alternative perturbation model. The group-specific loadings are generated as in Simulation case 3 Figure 14 shows the true and estimated loading matrices from BMFSA, FBPFSA and PFA across a range of values of α . The estimated loadings from PFA are much closer to the truth than BMFSA. We find that the estimated loading matrices are some permutation of the true loading matrix with some exceptions. For the cases with higher perturbation (row 2 and 4 of Figure 14), BMSFA estimates are in general not good. For the cases with higher perturbation, PFA estimates are bad for lower values of α . Similarly, for the cases with lower perturbations, PFA estimates with lower α are better than higher α estimated loadings. Table 10 compares predictive likelihoods of the two methods in different cases, and again, PFA and FBPFSA outperform BMSFA.

TABLE 10
Average predictive log-likelihood for PFA for different choices of α , FBPFSA and BMSFA in Simulation S.Case 1.

Generative Distribution of Ψ_j 's	True Loading	PFA for $\alpha = 1 \times 10^{-2}$	PFA for $\alpha = 1 \times 10^{-4}$	FBPFSA	BMSFA
N(-0.2, 0.2)	Loading 1	-56.27	-60.71	-56.63	-429.28
	Loading 2	-1041.28	-361.82	-421.28	-5853.65
N(-0.5, 0.8)	Loading 1	-30.68	-50.09	-54.62	-514.67
	Loading 2	-320.04	-246.06	-479.59	-6798.37

S.Case 2: Observation-level perturbations. In this case, we generate data from the model in (2.2). First, a non-perturbed dataset is generated exactly the same way as in Case 1 and 2. Then, we generate separate perturbation matrices $Q_{i0} \sim \text{MN}(I_p, \alpha_0 I_p, \alpha_0 I_p)$ for each data vector Y_i . We repeat this simulation for different choices of α_0 .

Figures 15 and 16 show the estimated loading when they are estimated using $\alpha = 1 \times 10^{-4}$. The method performs poorly when perturbation parameter α is lower than true parameter α_0 as in the previous cases. Figure 17 illustrates performance of FBPFSA in this case. When perturbation is higher, the performance deteriorates as it is more difficult to capture the loading structure accurately. Overall, our method is able to accurately estimate the true loading structure under some permutation of the columns.

More exploratory analysis on NHANES data. For each chemical level, we fit an one-way ANOVA model to analyse group-specific effects on each phthalate level separately.

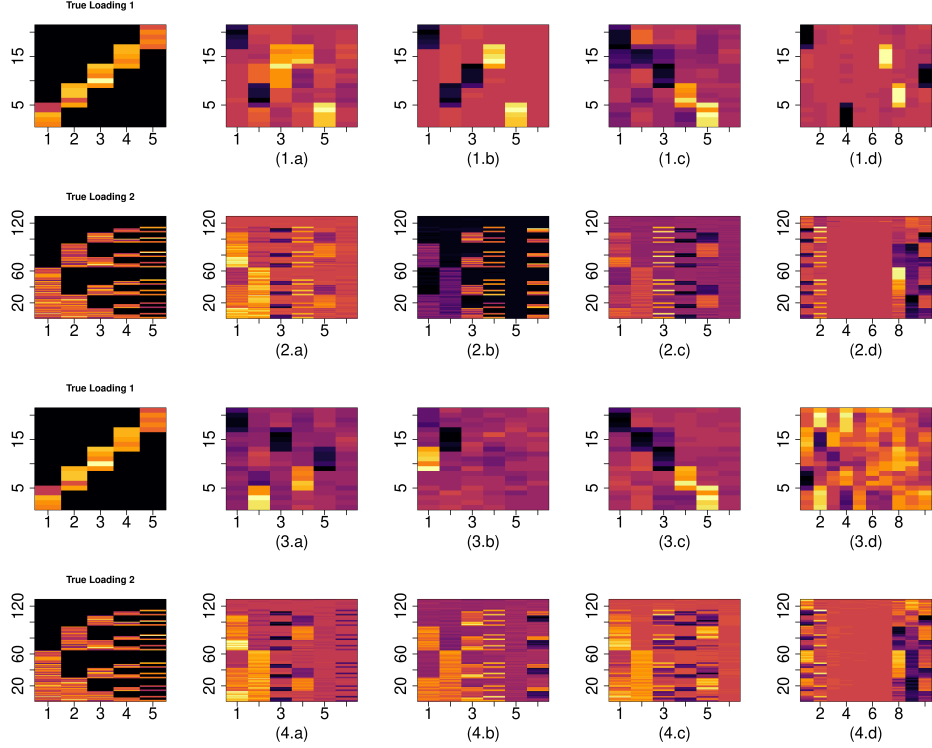
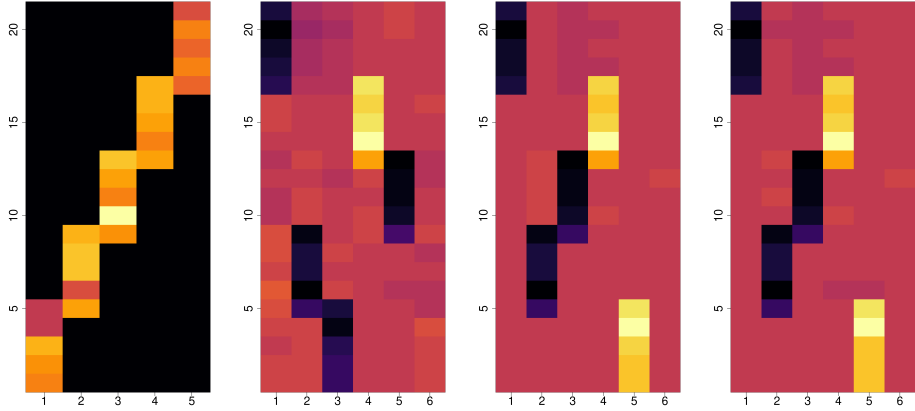
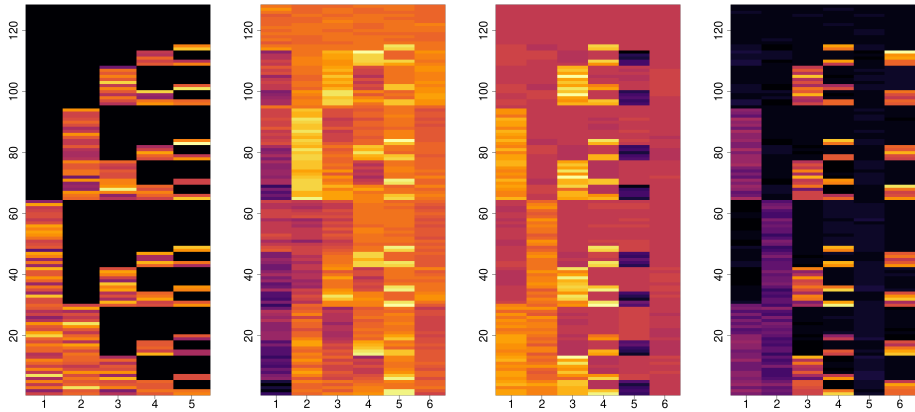


FIG 14. Comparison of estimated loading matrices in Simulation S. Case 1 with different choices of α for both of the two choices of loadings when group specific perturbations are added to the shared loading matrix by addition. The first two rows true Ψ_j 's are generated from $N(-0.2, 0.2)$ and for the last two rows Ψ_j 's are generated from $N(-0.5, 0.8)$ (a) Estimated loading for $\alpha = 1 \times 10^{-2}$, (b) Estimated loading for $\alpha = 1 \times 10^{-4}$, (c) Estimated loading for FBPFA, (d) Estimated loading from BMSFA



(a) The true loading matrix (b) Loading when $d = 100$ and $\alpha = 0.01$ (c) Estimated loading when $d = 100$ and $\alpha = 0.0001$ (d) Loading when $d = 100$ and $\alpha = 0.00001$

FIG 15. Comparison of the estimated loading matrices in Simulation S.Case 4 for observation level perturbation with different choices of hyperparameter d and different true perturbation parameter α_0 , where $Q_{i0} \sim MN(I_p, \alpha_0 I_p, \alpha_0 I_p)$ and $\alpha_0 = 1 \times 10^{-4}$ when the true loading is Loading 1.



(a) The true loading matrix (b) Loading when $d = 100$ and $\alpha = 0.01$ (c) Estimated loading when $d = 100$ and $\alpha = 0.0001$ (d) Loading when $d = 100$ and $\alpha = 0.00001$

FIG 16. Comparison of the estimated loading matrices in Simulation Case 4 for different prior choices of d and different true perturbation matrices Q_{i0} , where $Q_{i0} \sim MN(I_p, \alpha_0 I_p, \alpha_0 I_p)$ and $\alpha_0 = 1 \times 10^{-4}$ when the true loading is Loading 2.

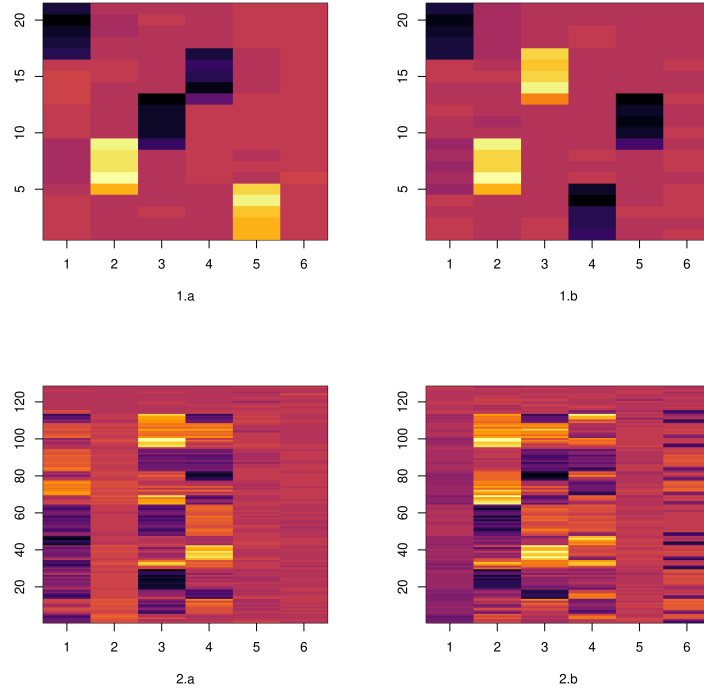


FIG 17. Estimated loadings using FBPFA for different choices of α_0 in Simulation Case 4 for two cases and two loadings. (a): Estimated loading for $\alpha_0 = 1 \times 10^{-4}$, (b): For $\alpha_0 = 1 \times 10^{-2}$.

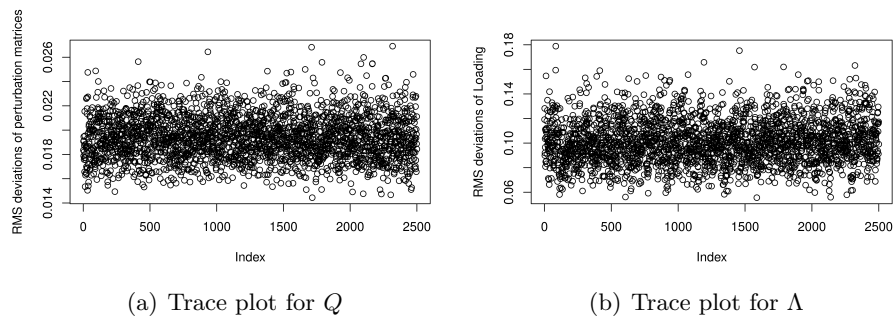


FIG 18. Trace plots of root mean square (RMS) deviations across the MCMC chain for the perturbation matrices and the shared loading matrix Λ .

TABLE 11
For *phthalate MnBP*

	Estimate	Std. Error	t value	Pr(> t)
(Intercept)	3.85	0.11	36.27	0.00
N-H Black	0.36	0.15	2.33	0.02
N-H White	-0.29	0.13	-2.26	0.02
OH	0.46	0.18	2.55	0.01
Other/Multi	-0.09	0.22	-0.41	0.68

TABLE 12
For *phthalate MiBP*

	Estimate	Std. Error	t value	Pr(> t)
(Intercept)	2.88	0.06	49.23	0.00
N-H Black	0.59	0.08	6.97	0.00
N-H White	-0.35	0.07	-4.98	0.00
OH	0.33	0.10	3.28	0.00
Other/Multi	-0.08	0.12	-0.68	0.50

ARKAPRAVA ROY
DEPARTMENT OF BIostatISTICS
UNIVERSITY OF FLORIDA
GAINESVILLE, FL
E-MAIL: ark007@phhp.ufl.edu

ISAAC LAVINE
AMY HERRING
DAVID B. DUNSON
DEPARTMENT OF STATISTICAL SCIENCE
DUKE UNIVERSITY
DURHAM, NC
E-MAIL: isaac.lavine@duke.edu
amy.herring@duke.edu
dunson@duke.edu

TABLE 13
For phthalate MEP

	Estimate	Std. Error	t value	Pr(> t)
(Intercept)	8.32	0.29	28.80	0.00
N-H Black	2.84	0.42	6.79	0.00
N-H White	-1.41	0.35	-4.02	0.00
OH	1.18	0.49	2.40	0.02
Other/Multi	-0.99	0.60	-1.64	0.10

TABLE 14
For phthalate MBeP

	Estimate	Std. Error	t value	Pr(> t)
(Intercept)	2.79	0.07	39.90	0.00
N-H Black	0.27	0.10	2.66	0.01
N-H White	-0.09	0.08	-1.05	0.29
OH	-0.01	0.12	-0.06	0.95
Other/Multi	-0.23	0.15	-1.57	0.12

TABLE 15
For phthalate MECPP

	Estimate	Std. Error	t value	Pr(> t)
(Intercept)	4.80	0.12	41.52	0.00
N-H Black	-0.44	0.17	-2.63	0.01
N-H White	-0.64	0.14	-4.56	0.00
OH	-0.25	0.20	-1.28	0.20
Other/Multi	-0.46	0.24	-1.89	0.06

TABLE 16
For phthalate MEHHP

	Estimate	Std. Error	t value	Pr(> t)
(Intercept)	3.83	0.10	36.85	0.00
N-H Black	-0.04	0.15	-0.26	0.79
N-H White	-0.39	0.13	-3.06	0.00
OH	-0.10	0.18	-0.56	0.58
Other/Multi	-0.26	0.22	-1.19	0.23

TABLE 17
For phthalate MEOHP

	Estimate	Std. Error	t value	Pr(> t)
(Intercept)	3.11	0.08	39.04	0.00
N-H Black	-0.06	0.12	-0.54	0.59
N-H White	-0.33	0.10	-3.39	0.00
OH	-0.11	0.14	-0.83	0.41
Other/Multi	-0.26	0.17	-1.54	0.12

TABLE 18
For phthalate MEHP

	Estimate	Std. Error	t value	Pr(> t)
(Intercept)	1.58	0.04	35.44	0.00
N-H Black	0.03	0.06	0.44	0.66
N-H White	-0.25	0.05	-4.57	0.00
OH	0.01	0.08	0.10	0.92
Other/Multi	0.00	0.09	0.02	0.99